Computer Methods in Biomechanics and Biomedical Engineering

ISSN: (Print) (Online) Journal homepage: https://www.tandfonline.com/loi/gcmb20

Assessing turbulent effects in ascending aorta in presence of bicuspid aortic valve

Rukiye Kara & Christian Vergara

To cite this article: Rukiye Kara & Christian Vergara (10 Nov 2023): Assessing turbulent effects in ascending aorta in presence of bicuspid aortic valve, Computer Methods in Biomechanics and Biomedical Engineering, DOI: 10.1080/10255842.2023.2279938

To link to this article: https://doi.org/10.1080/10255842.2023.2279938

Published online: 10 Nov 2023.

COMPUTER METHODS IN BIOMECHANICS AND BIOMEDICAL ENGINEERING
https://doi.org/10.1080/10255842.2023.2279938

Assessing turbulent effects in ascending aorta in presence of bicuspid aortic valve

Rukiye Kara[a] and Christian Vergara[b]

[a]Department of Mathematics, Mimar Sinan Fine Arts University, Istanbul, Turkey; [b]LABS - Dipartimento di Chimica, Materiali e Ingegneria Chimica" Giulio Natta" - Politecnico di Milano, Milan, Italy

ABSTRACT

Aortic valves with bicuspids have two rather than three leaflets, which is a congenital heart condition. About 0.5–2% of people have a bicuspid aortic valve. Blood flow through the aorta is commonly believed to be laminar, although aortic valve disorders can cause turbulent transitions. Understanding the impact of turbulence is crucial for foreseeing how the disease will progress. The study's objective was use large eddy simulation to provide a thorough analysis of the turbulence in bicuspid aortic valve dysfunction. Using a large eddy simulation, the blood flow patterns of the bicuspid and tricuspid aortic valves were compared, and significant discrepancies were found. The velocity field in flow in bicuspid configurations was asymmetrically distributed toward the ascending aorta. In tricuspid aortic valve (TAV) the flow, on the other hand, was symmetrical within the same aortic segment. Moreover, we looked into standard deviation, Q-criterion, viscosity ratio and wall shear stresses for each cases to understand transition to turbulence. Our findings indicate that in the bicuspid aortic valve (BAV) case, the fluid-dynamic abnormalities increase. The global turbulent kinetic energy and time-averaged wall shear stress for the TAV and BAV scenarios were also examined. We discovered that the global turbulent kinetic energy was higher in the BAV case compared to TAV, in addition to the increased wall shear stress induced by the BAV in the ascending aorta.

ARTICLE HISTORY
Received 25 January 2023
Accepted 30 October 2023

KEYWORDS
Blood flow; transition to turbulence; bicuspid aortic valve; large eddy simulation

1. Introduction

The aortic valve has commonly three leaflets; however, $0.5-2\%$ of new-born has only two leaflets due to fusion of two of them, which is referred to as congenital bicuspid aortic valve (BAV) disease. Bicuspid aortic valve (BAV) is the most frequent congenital cardiac disfigurement. It is often associated to ascending aortic dilation or even aneurysm. Indeed, the dilatation of ascending aorta and aneurysm when compared with patients with a normally functioning tricuspid aortic valve (TAV) is an higher risk for BAV cases (Hahn et al. 1992; Fedak et al. 2002). Furthermore, approximately 75% of BAV cases, who are more than 40 years old, have associated aneurysmal dilatation on the ascending aorta (Cecconi et al. 2005). An ascending aortic disease characterized by a predisposition to the aortic aneurysm, which may lead to aortic dissection, is the most frightening complication and affect 33% of BAV patients. Aortic dissection, rupture and sudden death due to severe enlargement of the aorta is also common (Sievers and Sievers 2011).

Flow pattern difference between bicuspid and tricuspid aortic valves into ascending aorta has been presented in recent in-vitro experimental studies (Seaman et al. 2014; Saikrishnan et al. 2015; McNally et al. 2017). Relation between aortic dilation and asymmetric jet flow was shown in Mahadevia et al. (2014) using MRI results and data analysis techniques.

In this respect, computational fluid dynamics (CFD) has been shown to be an effective tool to study flow patterns in BAV patients. Flow characteristics and variations in ascending aorta between BAV and TAV are demonstrated by using several computational fluid dynamics (Conti et al. 2010; Viscardi et al. 2010; Vergara et al. 2012; Chandran and Vigmostad 2013; Marom et al. 2013; Pasta et al. 2013; Faggiano et al. 2013a; Cao et al. 2017; Cao and Sucosky 2017; Kimura et al. 2017). Examples of computational studies in patient-specific geometries and

CONTACT Rukiye Kara rukiye.kara@msgsu.edu.tr

data are: the comparison between TAV and BAV models using finite element methods to analysis effects of higher stresses on leaflets (Conti et al. 2010) and distribution of Wall Shear Stresses (WSS) (Viscardi et al. 2010; Pasta et al. 2013; Kimura et al. 2017); the variations of WSS for non-fused cups with different angle for BAV cases in comparison with healthy TAV (Jermihov 2011; Vergara et al. 2012); the comparison with results obtained by in-vitro models (Chandran and Vigmostad 2013) and PC-MRI data (Faggiano et al. 2013a; Wendell et al. 2016); CFD studies on group of patients with different BAV pathologies investigating flow hemodynamics with respect to clinical evidence (Youssefi et al. 2017). Notably, blood flow has been seen to have specific properties for BAV cases such as eccentric flow jets, high concentrated WSS, helical flow, and elevated retrograde flows in ascending aorta, particularly exhibiting abnormalities in dilated BAV (Viscardi et al. 2010; Barker et al. 2012; Chandra et al. 2012; Bissell et al. 2013; Pasta et al. 2013; Mahadevia et al. 2014; Seaman et al. 2014; Burris and Hope 2015; van Ooij et al. 2015; Cao et al. 2017; Kimura et al. 2017; Oliveira et al. 2019).

Characteristics of blood flow play an important role in cardiovascular studies, since the correct definition and evaluation of these features are fundamental in understanding diseases and treatment process (Steinman 2002; Kheradvar and Pedrizzetti 2012). To this end, turbulence or transition to turbulence and velocity fluctuations in the aorta of animals and humans have been studied *in vivo*, some of which yielded fully developed turbulence in ascending aorta (Nerem and Seed 1972; Stein and Sabbah 1976; Nygaard et al. 1994; Fortini et al. 2015). Blood flow turns into turbulence in the ascending aorta, especially during the deceleration phase and in presence of pathophysiological effects such as narrowing, high curvature and enlargement of lumen (Gülan et al. 2016). Disturbed flow in the ascending aorta was observed also along the systole, even in healthy cases (Stein and Sabbah 1976). Complex fluid dynamics such as vortices, retrograde and asymmetrical jet flow are characterized by a disturbed flow and possible transition to turbulence. These properties were observed *in vitro* and vivo studies (Hope et al. 2010, 2011; Morbiducci et al. 2011). In subjects with aortic disease, flow displays this kind of turbulence properties in the ascending aorta (Fortini et al. 2015) and turbulence fluctuation can cause to influence WSS, which is related to arterial wall degradation, especially in bicuspid aortic valve (Davies et al. 1986; Barker et al. 2012). Moreover, TAV and BAV cases were compared with respect to the level of turbulence *via* particle image velocimetry experiments (Saikrishnan et al. 2015).

To figure out the effects of turbulence on the aortic wall of BAV cases, CFD has been used to predict transitional blood flow patterns. In order to investigate all properties of turbulent flow, computational costs need to be reduced in complex geometries with turbulent flow, although direct numerical simulation (DNS) which resolves all scales is the most precise method. As to understand effects of turbulent fluctuations, a turbulence model comes as reasonable method. In Reynolds Averaged Navier-Stokes (RANS) equations a time-averaged solution of the flow is obtained, however some certain absent dynamics of the flow will limit the representations. $k-\omega$, RNG $k-\epsilon$ and standard $k-\epsilon$ models have been commonly performed in aorta (Benim et al. 2016; Zhang et al. 2018; Trigui et al. 2021).

On the other hand Large Eddy Simulation (LES) is a reliable tool to model turbulence effects, which relies on a coarse mesh that models small scale effects. In this method, flow dynamics can still be analyzed with less computational cost. LES is widely performed for turbulent flow through an application of a filter which separates velocity field into two parts called resolved and unresolved, that represent large eddies and subgrid scales (Kara and Çağlar 2018). Varghese et al. (2008) and Tan et al. (2011) investigated flow properties using idealized geometries such as circular stenosed pipe. Also, Gårdhagen et al. (2010) examined WSS in the same type of geometry. Lantz et al. (2012) used LES with WALE subgrid scale model to qualify WSS in human specific aorta. Specifically for the hemodynamic case, LES with eddy-viscosity σ-model has been proposed in Nicoud et al. (2011), with applications, e.g. to the ventricular blood dynamics (Chnafa et al. 2016; Bennati et al. 2023) and the abdominal aortic aneurysms (Vergara et al. 2017).

Turbulence level is expected to increase in BAV patients, as well as eccentric and helical flow and higher WSS in the ascending aorta are observed. There are only a few studies in the literature that investigate turbulent flow dynamics in BAV cases. Hsu et al. (2011) considered mechanical bicuspid aortic valve and examined hemodynamics of flow using RANS method. Xu et al. (2020) employed the LES method with WALE model in RL-BAV case using mesh with around 6 million elements.

In this work, we presented a study where blood dynamics in TAV and BAV cases built in the same geometry were compared to assess the different amount of turbulence experienced by the two scenarios and induced by the different leaflets configurations. We used the LES σ− model (Nicoud et al. 2011) and we analyzed relevant quantities such as standard deviation of solutions among different heartbeats, subgrid eddy viscosity, Q-criterion, global turbulent kinetic energy, and wall shear stresses. The main novelties of this work consist in the inclusion of the aortic valve leaflets in a comparison between turbulence effects developed by TAV and BAV cases and of variations of blood velocity among heartbeats to quantify the developed turbulence.

2. Methods

2.1. Geometric pre-processing

In this study, we used the computational geometries set up in Bonomi et al. (2015). In particular, we started from a 3D contrast-enhanced MRI (CE-MRI) image with a voxel resolution of $1.72 \times 1.72 \times 1.5$ mm of a BAV patient, with no aortic dilation nor valve stenosis. A level set segmentation technique implemented in the open source code Vascular Modeling Toolkit (vmtk, http://www.vmtk.org) was utilized to create a surface model of the patient's aortic root, ascending aorta, and aortic arch from MRI data. Then, starting from this model, we built up two different configurations, a TAV and a BAV one. To generate the two configurations, we followed the strategy reported in Conti et al. (2010), where valve orifice areas, leaflet insertion lengths, valsalva sinus profiles, and ascending aorta positions were determined using MRI data from 10 TAV and 8 BAV healthy patients. This allowed the authors to generate average TAV and BAV leaflets model geometries which were included in the computational domain. The open position of the leaflets were obtained by using two structural simulations (Conti et al. 2010). Mechanical properties of leaflets used for such structural simulations were transversely isotropic incompressible hyperelastic and were modeled by the strain energy function

$$W = c_0 \exp\left(c_1(I_1 - 3)^2 + c_2(I_4 - 1)^2 - 1\right), \qquad (1)$$

where I_1 and I_4 are the first and fourth invariants of the Cauchy–Green strain tensor. Constants c_0, c_1, c_2 were set by fitting with the model reported by Billiar and Sacks (2000). Strain energy function (1) was implemented into the ABAQUS/Explicit code with a VUMAT subroutine. Notice that these structural simulations performed in Conti et al. (2010) were used in Bonomi et al. (2015) and here only to obtain the open and close configurations of the TAV and BAV leaflets to be included in the fluid domain. No fluid-structure interactions simulations were performed in the present work.

The open configurations of the average BAV and TAV cases were then mapped into the volume of the patient, so that the dimensions of the BAV orifice and the valve orientation were the same as the TrueFisp measurements, i.e. $2.0\,\mathrm{cm}^2$. For the TAV case we assumed an orifice area of $3.1\,\mathrm{cm}^2$, see Bonomi et al. (2015). Afterwards, a volume mesh of linear tetrahedra was generated with vmtk for the fluid domain with the presence of the leaflets (Bonomi et al. 2015). For further details, we refer the reader to Conti et al. (2010) and Bonomi et al. (2015).

2.2. The mathematical model

In large and medium vessels, blood flow, which is modeled as an incompressible, homogeneous, and Newtonian fluid, is governed by incompressible Navier-Stokes equations (NSE) with constant density in the domain Ω. Although not negligible in the aorta, we neglect is this work the vessel compliant and we rely on rigid wall simulations. Defining the unknown velocity field $\mathbf{u}(\mathbf{x}, t) : \Omega \times [0, T] \to \mathbb{R}^3$ and pressure field $p(\mathbf{x}, t) : \Omega \times [0, T] \to \mathbb{R}$ in absence of body forces, the NSE, which provide continuity and momentum conservation equations, read as follows:

$$\begin{gathered} \frac{\partial \mathbf{u}}{\partial t} - \nu \nabla \cdot \mathbf{S}(\mathbf{u}) + \nabla \cdot (\mathbf{u} \otimes \mathbf{u}) + \nabla p = \mathbf{0} \\ (\mathbf{x}, t) \in \Omega \times (0, T], \ \nabla \cdot \mathbf{u} = \mathbf{0} \quad (\mathbf{x}, t) \in \Omega \times (0, T], \end{gathered} \qquad (2)$$

where ν is the kinematic viscosity, $[\mathbf{u} \otimes \mathbf{u}]_{ij} = u_i u_j$ and $\mathbf{S}(\mathbf{u}) = \nabla \mathbf{u} + (\nabla \mathbf{u})^T$.

In computational fluid dynamics, the large eddy simulation (LES) is a mathematical model for turbulence, that has reduced computational cost for high Reynolds numbers (Sagaut and Meneveau 2006). Flow variables are decomposed into resolved (filtered) and unresolved subgrid scale terms for this method's basis. The velocity and pressure fields can be decomposed as $\mathbf{u} = \bar{\mathbf{u}} + \mathbf{u}'$ and $p = \bar{p} + p'$ where $\bar{\mathbf{u}}(\mathbf{x}, t) = \int_{-\infty}^{\infty} \mathbf{u}(\xi, t) G(\mathbf{x} - \xi) d^3\xi$ is the filtered velocity field in space and G is the filter function with length $\bar{\Delta}$ that determines the size and structure of the small scales. Applying the filter function (virtually) to the

Navier-Stokes equations for incompressible flows, the filtered Navier-Stokes equations are obtained as

$$\frac{\partial \bar{\mathbf{u}}}{\partial t} - \nu \nabla \cdot \mathbf{S}(\bar{\mathbf{u}}) + \nabla \cdot (\bar{\mathbf{u}} \otimes \bar{\mathbf{u}}) + \nabla \bar{p} + \nabla \cdot \boldsymbol{\tau}^{\boldsymbol{d}}(\bar{\mathbf{u}}) = 0$$
$$(\mathbf{x}, t) \in \Omega \times (0, T], \quad \nabla \cdot \bar{\mathbf{u}} \quad = 0 \quad (\mathbf{x}, t) \in \Omega \times (0, T], \tag{3}$$

where $\boldsymbol{\tau} = \overline{\mathbf{u}\mathbf{u}} - \bar{\mathbf{u}}\,\bar{\mathbf{u}}$ is the subgrid scale tensor which is modeled to represent the effect of small scales and $\boldsymbol{\tau}^{\boldsymbol{d}}$ is its deviatoric part. In particular, in eddy viscosity models one introduces a suitable subgrid viscosity ν_t and build accordingly the subgrid scale tensor as follows:

$$\boldsymbol{\tau}^{d} = \nu_t(\nabla \mathbf{u} + (\nabla \mathbf{u})^T).$$

In this study, we consider the σ-model, a subgrid scale model introduced for enclosed fluids (Nicoud et al. 2011), which is based on the singular values of the resolved velocity gradient tensor. With $\sigma_1(\mathbf{x}, t) \geq \sigma_2(\mathbf{x}, t) \geq \sigma_3(\mathbf{x}, t) > 0$ being the singular values of $\nabla \bar{\mathbf{u}}$, the σ-model is given by the following eddy viscosity:

$$\nu_t = C_\sigma \bar{\Delta}^2 \left(\frac{\sigma_3(\sigma_1 - \sigma_2)(\sigma_2 - \sigma_3)}{\sigma_1^2} \right), \tag{4}$$

where C_σ is a suitable constant and $\bar{\Delta}$ the filter width.

Moreover, a suitable initial condition for system (3), $\bar{\mathbf{u}}(\mathbf{x}, 0) = \bar{\mathbf{u}}_0(\mathbf{x})$, and boundary condition for $\forall t > 0$

$$\begin{aligned} \bar{\mathbf{u}}(\mathbf{x}, t) &= \boldsymbol{\phi}(\mathbf{x}, t), \quad \mathbf{x} \in \Gamma_D, \\ (-\bar{p}\mathbf{n} + \nu \mathbf{S}(\bar{\mathbf{u}})\mathbf{n} - \boldsymbol{\tau}^{\mathbf{d}}(\bar{\mathbf{u}})\mathbf{n})(\mathbf{x}, t) &= \mathbf{0}, \quad \mathbf{x} \in \Gamma_N, \end{aligned} \tag{5}$$

where $\bar{\mathbf{u}}_0$ is given vectorial functions, and ϕ is velocity boundary data, Γ_D and Γ_N are portions of the domain border $\partial\Omega$ of Ω such that $\Gamma_D \cup \Gamma_N = \partial\Omega, \Gamma_D \cap \Gamma_N = \emptyset$, where Γ_D is the inlet, Γ_N the four outlets of the ascending aorta, and $\mathbf{n}$ is the outgoing normal vector of $\partial\Omega$. Model coefficient C_σ is taken to equal to 1.5 for blood flow (Lancellotti et al. 2017; Vergara et al. 2017).

2.3. Description of the numerical simulations

In this study, two different patient-specific ascending aortic valves without stenosis are analyzed in BAV and TAV models with leaflets. Surface models of the two configurations has been transformed to computational mesh using with the open-source code Vascular Modeling Toolkit (vmtk, http://www.vmtk.org). Mesh refinement is employed by boundary layer resolution applied to the grid near wall boundaries to well describe WSS variation and turbulence properties for both cases. Large eddy simulation with static σ-model is used for numerical simulation on reconstructed geometries. At the inflow section Γ_D a flat velocity profile was applied (Moireau et al. 2012) to prescribe the representative flow rate (obtained from the velocity curves reported in Avolio (1980) by multiplication with the cross section area) reported in Figure 1. However, it is important to note that we made an adjustment to the flow curve to suit our computational simulations. Specifically, we removed the negative portion of the curve and adjusted it to nullify negative values. This modification was implemented to account for the ascending aortic flow rate which is usually positive. We notice that the systolic/diastolic split is a little bit large; since our analysis was mainly focused in the systolic phase and since the flow rate is null in the last part of the diastolic phase, we believe that this approximation should not affect so much our results, especially since they represent comparisons so that all configurations are in the same framework. A zero-stress condition was imposed at the outlets of interest region in the ascending aorta with no-slip wall conditions on the rigid wall boundaries. The opening/closure of the aortic valve (both TAV and BAV cases) was modeled through an on/off modality: the open configuration (leaflets included in the fluid domain) is considered during the systolic phase, when the prescribed flow rate is greater than zero, whereas the closed configuration is considered during diastole.

LES is carried out *via* the open-source finite element library LifeV (Bertagna et al. 2017). This is designed in C++ and offers a variety of tools and algorithms for simulating complicated physical processes in a number of different areas, such as biomechanics, fluid-structure interaction, and cardiovascular mechanics. Time discretization was performed using second order backward differentiation formula (BDF2). Also P1-P1 finite elements were used with SUPG-PSPG and backflow stabilization techniques.

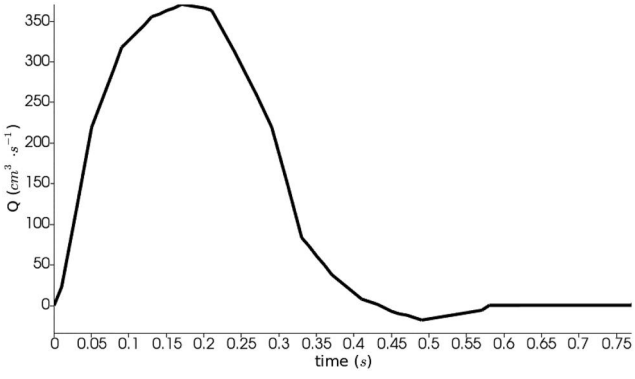

Figure 1. Flow rate prescribed at the inlet for aortic valve with leaflets. Taken from (Avolio 1980).

Blood density ρ of 1.0 g/cm^3 and kinematic viscosity ν of 0.035 Poise were used. We ran five heartbeats and we discharged the first one, so that the ensemble quantities and the standard deviation (see Sect. 2.4) were computed over four heartbeats. The period was set $T = 0.77s$.

2.4. Quantities of interest

To characterize blood flow and transition to turbulence, some post-processing quantities are considered:

- **Ensemble Average.** If $\psi(t,\mathbf{x})$ is given quantities defined over several periods of equal length T, the ensemble-average of $\psi(t,\mathbf{x})$ is defined as

$$< \psi(t,\mathbf{x}) >= \frac{1}{M}\sum_{j=1}^{M}\psi(t+(j-1)T,\mathbf{x}), \quad t \in (0,T]$$

where M is the number of heartbeats ($M=4$ in our case). With the ensemble average, deviation of the interest field from its mean is ignored. In this study, we consider the ensemble average of velocity magnitude U, wall shear stress magnitude WSS, and time averaged wall shear stress $TAWSS$, where

$$U(t,\mathbf{x}) = ||\bar{\mathbf{u}}(t,\mathbf{x})||_{\mathbb{R}^3}, \quad t \in (0,MT],$$
$$WSS(t,\mathbf{x}) = \nu\sqrt{\sum_{j=1}^{2}((\nabla\bar{\mathbf{u}}\ \ \mathbf{n})\cdot\tau^{(j)})^2}, \quad t \in (0,MT],$$
$$TAWSS(\mathbf{x}) = \frac{1}{T}\int_0^T ||WSS(t,\mathbf{x})||\ dt,$$

where $\mathbf{n}$ is the outward unit vector and $\tau^{(j)}, j = 1,2$, the tangential unit vectors.

Standard Deviation. Standard deviation of velocity fluctuation is defined as

$$< SD(t,\mathbf{x}) >=$$
$$\sqrt{\frac{1}{M}\sum_{j=1}^{M}\left(U(t+(j-1)T,\mathbf{x}) - < U(t,\mathbf{x}) >\right)^2} \quad t \in (0,T].$$

High values of standard deviation indicate large turbulence levels in the flow. This allows us to quantify and localize the velocity fluctuations and thus transition to turbulence.

Global Turbulent Kinetic Energy. To analyze the global degree of velocity fluctuations, $GTKE(t)$ is defined as space integral of turbulent kinetic energy

$$GTKE(t) = \int_\Omega TKE(t,\mathbf{x})\ d\mathbf{x}, \quad t \in (0,T],$$

where

$$TKE((t,\mathbf{x}) = \frac{1}{2M}\sum_{j=1}^{M}(\bar{u}_x(t+(j-1)T,\mathbf{x}) - < u_x(t,\mathbf{x}) >)^2 +$$
$$+(\bar{u}_y(t+(j-1)T,\mathbf{x}) - < u_y(t,\mathbf{x}) >)^2 +$$
$$+(\bar{u}_z(t+(j-1)T,\mathbf{x}) - < u_z(t,\mathbf{x}) >)^2) \quad t \in (0,T].$$

2.5. On the choice of discretization parameters

LES models allow to describe the turbulent characteristic of blood with a coarser mesh than the one needed by a DNS, where all turbulent scales are comprised. In LES, large scales of turbulent flow are computed directly, whereas small scales are modeled which reflect effects of unresolved scales that can not be captured by mesh. The choice of the mesh resolution for LES is thus of crucial point in order to have a good accuracy with reduced computational times. To do this, we performed a mesh convergence study. In particular, we selected the final mesh when, increasing the number of mesh points of a factor 10%, the solution did not change by a factor greater than 5%.

Technically, on the numerical solution of the problem, time discretization was performed using a semi-implicit approach for linearization the momentum equation, in combination with second order backward differentiation formula (BDF2) but a implicit approach in eddy viscosity terms. Time discretization parameter was taken equal to $\Delta t = 0.01s$ with guaranteed to time independence up to a proper value tolerance. In both cases, the mesh consisted of approximately 960k tetrahedral elements with the non-uniform mesh in which the grids had varying mesh size. Characteristic mean mesh size was taken equal to 0.09 mm in both cases. The meshes and leaflets are shown in Figure 2.

3. Numerical results

In this section, we report some numerical results obtained in the different scenarios (TAV and BAV) with the aim of analyzing the effect of a bicuspid valve on the evolution of disturbed flows and transition to turbulence.

The ensemble velocity magnitude in ascending aorta for the two different configurations is shown on the left side of Figure 3 at early systole, peak systole

and late systole phases. In all figures, upper row represents TAV and lower BAV. Skewness of velocity profiles of TAV models are nearly symmetrical during systole. Flow is mainly laminar which means streamlines aligned with the wall, and transition to turbulence do not occur in TAV case. Moreover, effects of leaflets are primarily observed with parallel flow profiles in BAV and TAV cases. In the BAV case, the flow progresses to an asymmetrical jet form oriented toward the aortic wall at the ascending aorta which is consistent with the flow patterns found in previous studies (Hope et al. 2010).

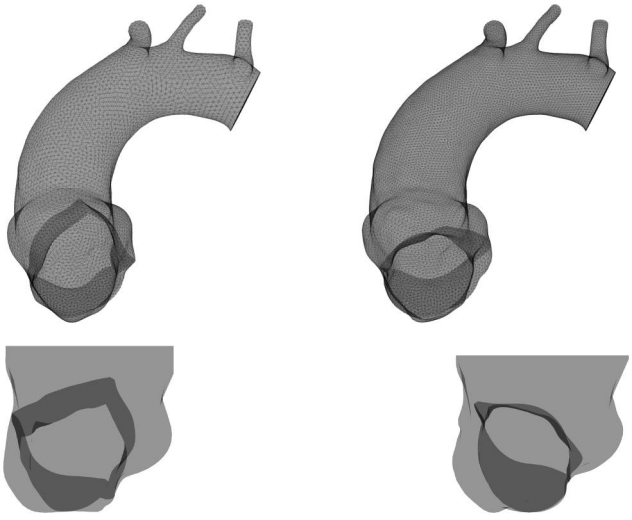

Figure 2. Mesh representing ascending aorta. The two valve leaflets models are also presented. Left: Mesh of the TAV case; Right: Mesh of the BAV case.

Q-criterion, which is useful for detecting vortex structures, defines the relative difference between strain rate and vorticity magnitude and is reported in the right portion of Figure 3 at the same three instants of above. Q-criterion could be used to visualize the disturbed flow. In the interest of determining a distinct separation between vortices, the value 5000 was used as the threshold for the Q-criterion visualization. This allowed us to make a distinction between coherent and incoherent turbulent flows. Our results show vortex structures colored by velocity. Due to the jet flow impact at the aortic wall, we observe complex vortex structures developing in BAV case in the ascending aorta during systole and also close to the wall during deceleration. The presence of vortical flows and variations of vortical magnitude in BAV were also observed by flow images by means of 4D MRI acquisitions (Hope et al. 2010).

In order to better assess the transition to turbulence developed in the bicuspid case, we analyze the viscosity ratio ν_t/ν in Figure 4, left, at the same three instants of above. This quantity gives information about the amount of subgrid viscosity introduced by the LES model in comparison with the physical viscosity. Large values of

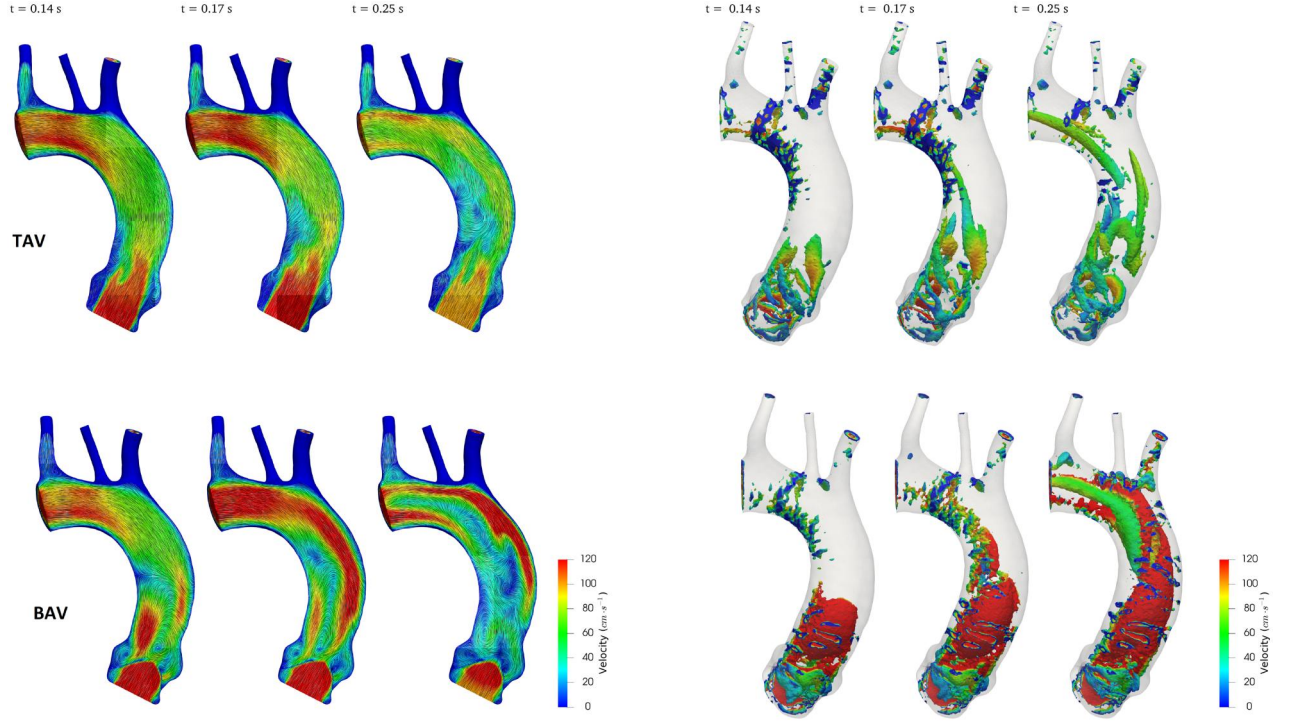

Figure 3. Left: Ensemble velocity magnitude. Right: Q-criterion (we report the regions with $Q > 5000$ painted by the ensemble velocity magnitude). Top: Results for TAV; Bottom: Results for BAV. Three time instants are reported for each case: Early systole $t = 0.14s$; peak-systole $t = 0.17s$; Late systole $t = 0.25s$.

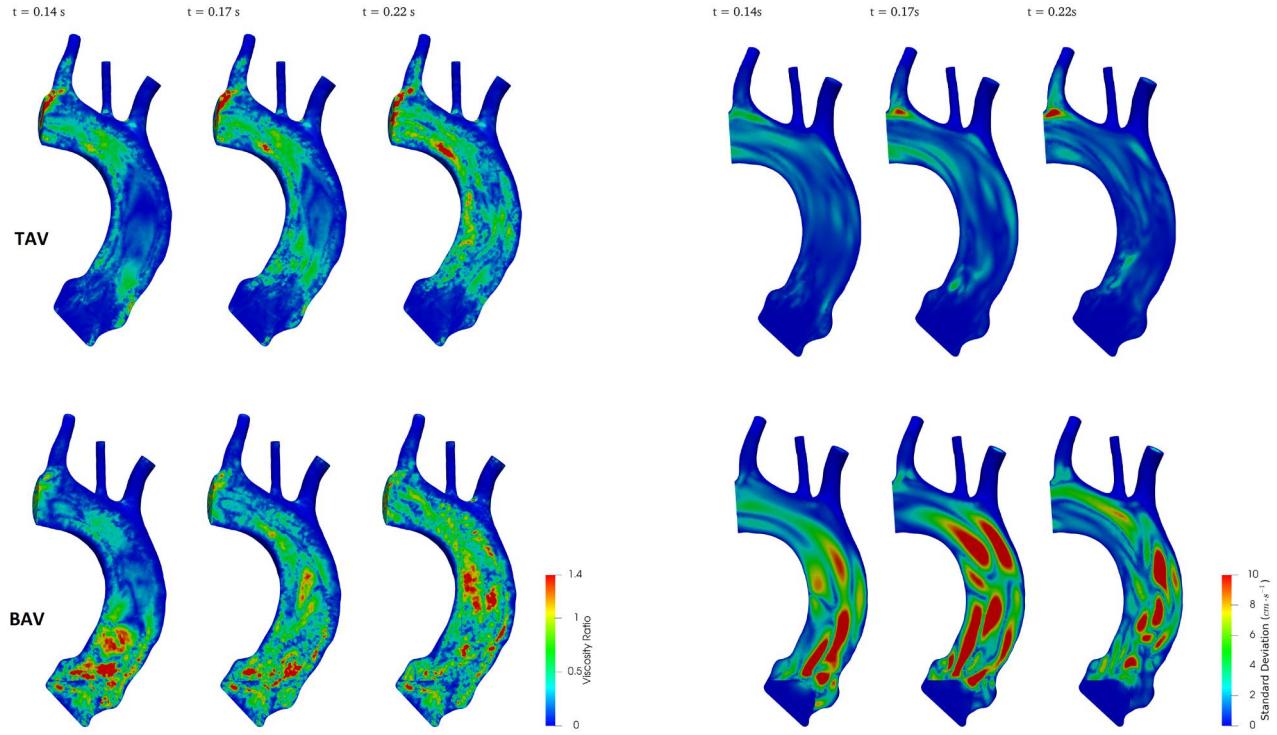

Figure 4. Left: Viscosity ratio, ratio between subgrid-scale and molecular viscosities. Right: Standard deviation of velocity field over the four heartbeats. Top: Results for TAV; Bottom: Results for BAV. Three time instants are reported for each case: Early systole $t = 0.14s$; peak-systole $t = 0.17s$; Late systole $t = 0.22s$.

Table 1. Percentage of some important quantities in all areas or volumes of the aortic valves considered.

Time	$t = 0.14s$		$t = 0.17s$		$t = 0.22s$		$t = 0.24s$	
Case	TAV	BAV	TAV	BAV	TAV	BAV	TAV	BAV
Viscosity Ratio > 1	0.7%	6.7%	1.4%	5.1%	2.9%	8.1%	3.0%	7.9%
WSS > 2.2 *Pa*	1.5%	9.7%	2.3%	15.8%	2.6%	22.8%	0.9%	22.9%
SD > 7	0.0%	13.5%	0.3%	18.6%	0.2%	8.2%	0.1%	4.8%

the viscosity ratio mean that the LES model highly works in terms of introducing subgrid terms and are indicators of a significant transition to turbulence. It is clear that blood flow in patients with BAV features significant turbulence development in comparison to the TAV case where this ratio is smaller. A high viscosity ratio in the center of aorta and sinotubular junction is observed as expected. Subgrid scale viscosity is found to be almost one and a half times greater than molecular viscosity and this in turn indicates that turbulence model is mainly active in BAV case. In Table 1, we report the percentage of volume (over the total volume in a region of interest) such that viscosity ratio is larger than 1 at different time instants. We notice that the volume exposed to 'high' values of viscosity ratio is about four times greater for BAV with respect to TAV and increases after peak-systole in both cases.

Another quantity that has been to see strictly related to the development of transition to turbulence is the standard deviation of the velocity field among the different heartbeats. This quantity allows to measure mean deviation of the velocity field along different heartbeats and indicates the presence of turbulent transition. Indeed, significant transition to turbulence is expected to lead to large velocity fluctuations, whereas completely laminar flows are expected to give null standard deviation. In the right part of Figure 4, standard deviation of velocity magnitude over four heartbeats at early systolic, peak-systolic and late systolic time instants are reported. We observe elevated velocity standard deviation for BAV case which corresponds to almost 10% of the velocity values (refer to bottom-right part of Figure 3). On the contrary, TAV case experiences almost null standard deviation. As seen in Table 1, percentage of volume where standard deviation is grater than $7cm \cdot s^{-1}$ is significant for BAV case (up to 18.65%), where it is almost zero for TAV case.

To reveal and interpret the effect of velocity on the wall, ensemble Wall Shear Stress (WSS) and the time averaged of ensemble Wall Shear Stress (TAWSS)

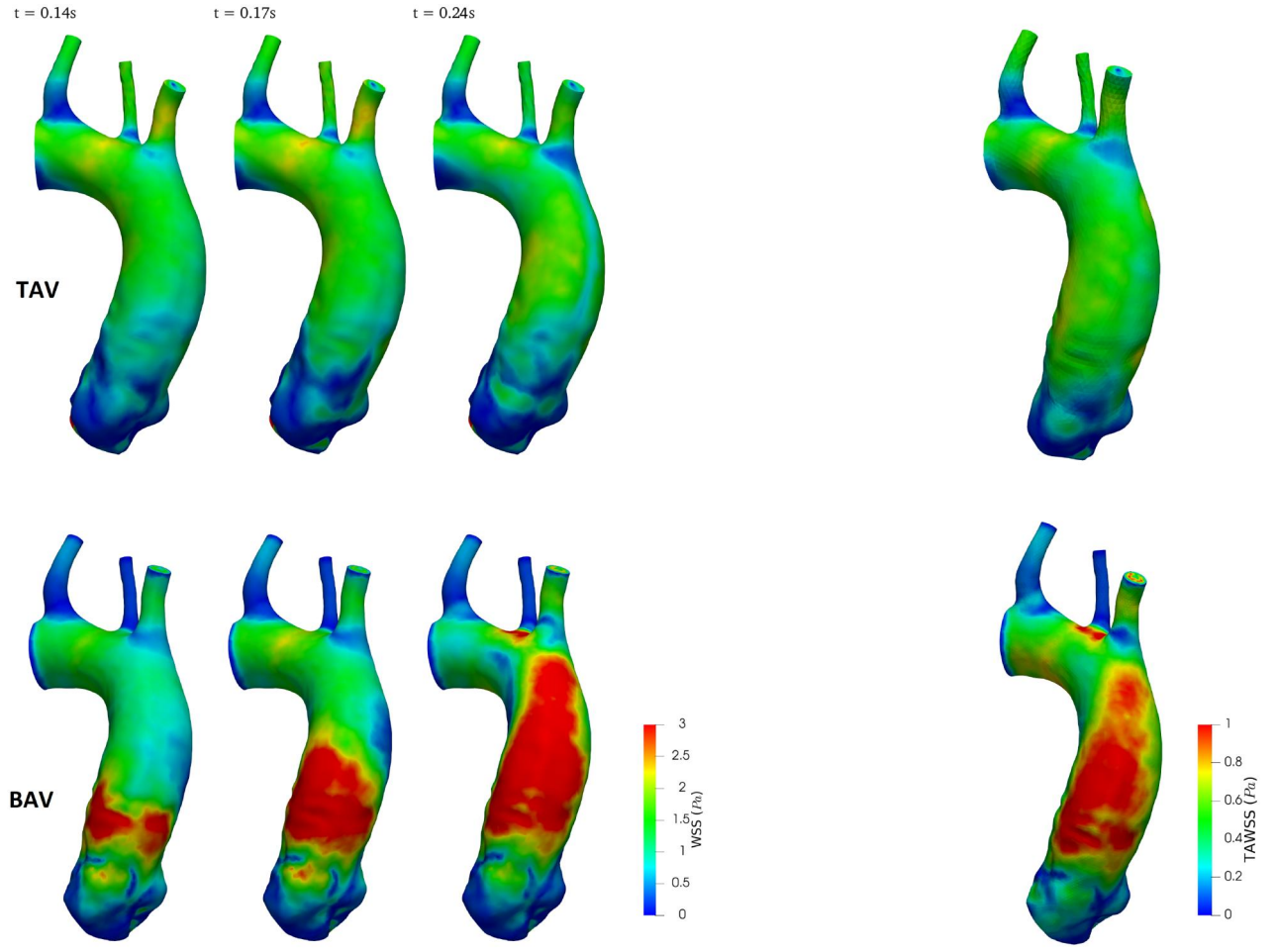

Figure 5. Left: Ensemble wall shear stresses. Three time instants are reported for each case: Early systole $t = 0.14s$; peak-systole $t = 0.17s$; Late systole $t = 0.24s$. Right: Time averaged of ensemble wall shear stresses. Top: Results for TAV; Bottom: Results for BAV.

distribution is shown in Figure 5. The significant differences between TAV and BAV are represented by increased WSS for BAV in the ascending aorta as a consequence of the impinging high velocity jet on the aortic wall. Also high TAWSS values occur for BAV along the curved side wall of ascending aorta, where the flow jet hits. In Table 1, the area percentage of WSS with a value greater than 2.2 *Pa* increases gradually after peak-systole in BAV. This value has been selected as representative of a possible cut-off between 'small' and' large' WSS since in the ascending aorta a common physiological range for WSS magnitude is given by (0.5, 2) Pa, see, e.g. Bissell et al. (2013) and Hope et al. (2010).

The Global Turbulent Kinetic Energy (GTKE) is analyzed in Figure 6 for TAV and BAV cases. It is clearly seen that the BAV case reaches its maximum value just after peak-systole, while the TAV is several times much lower. The maximum and mean values of GTKE for both cases is reported in Table 2. We observe that both values are significantly larger in the BAV case.

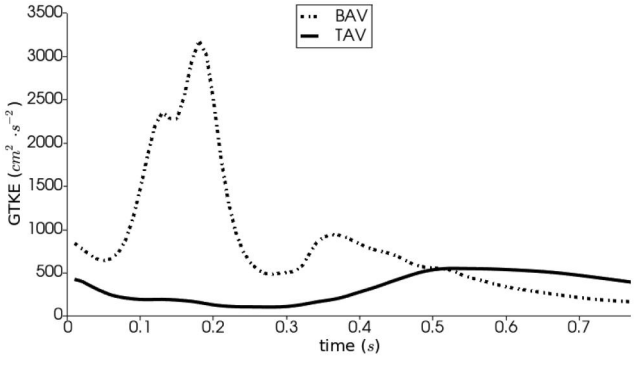

Figure 6. Global turbulent kinetic energy over four heartbeats for TAV (——) and BAV (— · —).

Table 2. Maximum and mean values of GTKE ($cm^2 \cdot s^{-2}$) in TAV and BAV cases.

Case	Maximum	Mean
TAV	548.5	327.2
BAV	3177.6	839.0

4. Discussion

Mathematical models and numerical simulations have been widely used for prediction of disease formation like ascending aortic aneurysm. Computational simulations, which are a very active area of research, can help us to better understand the underlying principles of the biomechanics of the aortic valve as well as BAV abnormalities. Computational modeling and analysis as methods for examining the biomechanical characteristics of the aortic valve can attain some quantities that is challenging to measure *in vitro* or *in vivo* experiments. Answering clinical questions of aortic aneurysm formation related to BAV using computational modeling with large eddy simulation is an unusual approach as evidenced by lack of literature to our knowledge. We proposed to provide a deeper perspective on ascending aorta in patients with TAV and BAV and carried out a computational study to investigate effects of BAV in a non dilated vessel. Fluid dynamics in the ascending aorta in presence of a bicuspid aortic valve was first investigated with CFD by Richards et al. (2004) in an ideal geometry without leaflet. One of the first patient-specific study was performed by Viscardi et al. (2010) in realistic geometry, where the leaflet was not modeled. Conti et al. (2010) analyzed the stresses on leaflets in an idealized geometry. On the other hand, Bonomi et al. (2015) examined the BAV and TAV cases by including the leaflet in realistic geometry.

Characteristic fluid dynamics such as the eccentric flow jet in the ascending aorta in patients with the BAV diseases were reported in several studies, both in-vivo and in the in-vitro studies (Conti et al. 2010; Seaman et al. 2014; McNally et al. 2017) whereas computational methods were performed many studies in patient specific geometries (Viscardi et al. 2010; Vergara et al. 2012; Chandran and Vigmostad 2013; Faggiano et al. 2013a; Kimura et al. 2017). Recently, fluid structure interaction studies in TAV and BAV cases have increased considerably (Moireau et al. 2012; Marom et al. 2013; Oliveira et al. 2019). Some authors analyzed of turbulence/transition effects on realistic geometries using turbulence models (Lancellotti et al. 2017; Xu et al. 2020).

Cardiovascular magnetic resonance (CMR) and CFD, that have been used by Guzzardi et al. (2015) and Torii et al. (2013) respectively, both have yielded similar results pointing to a correlation between WSS and ascending aorta shape such as dilation, as well as wall degeneration. Oliveira et al. (2019) analyzed the flow characteristics of blood on dilated BAV models with leaflet using FSI.

In the present study, skewed velocity profile and eccentric flow jet in blood flow are found in ascending aorta of BAV patient. We have also confirmed WSS distribution in both BAV configuration, which causes aneurysm formation. Although some vivo studies point to a higher hemodynamic stress in the ascending aorta in BAV patients with the stenotic condition (coarctation of aorta) than patient with stenotic TAV, we see that this is also applies to non-stenotic situations (Tadros et al. 2009; Nathan et al. 2011; Wittberg et al. 2016; Shan et al. 2017).

We also noticed for the BAV case elevated velocity and wall shear stress in the mid-ascending aorta. These observations are consistent with Malota's physical model results (Malota et al. 2013) and previous MRI reports (Barker et al. 2012; Bissell et al. 2013; Mahadevia et al. 2014). However, magnetic resonance imaging can not measure precisely WSS and evaluation is unreliable (Rinaudo and Pasta 2014). Hence, computational modeling is favorable.

Moreover increased WSS can be associated with turbulence and play an important role to BAV-related diseases. Turbulence characteristics come into view during early systole. These results can also be specified by standard deviation and high viscosity ratio in the center of aorta and sinotubular junction. The turbulent flow properties are more intense in BAV case than healthy case. Our simulation provide clear evidence that BAV models has a transition to turbulence. Recently some of the experimental studies considered to transitional and turbulent flow (Saikrishnan et al. 2015; Gülan et al. 2016; McNally et al. 2017; Ha et al. 2018).

The relevance of the turbulent study performed in this work is confirmed by some clinical studies highlighting that the turbulent flow may cause degenerative changes in the aortic wall in patients with bicuspid aortic valve, and that these degenerative processes are worse than in the tricuspid cases (de Sa et al. 1999; Girdauskas et al. 2011).

We highlight that the outcomes of this work refer to a non-stenotic BAV analysis. Indeed, we wanted to evaluate whether the mere presence of a BAV orifice was responsible for the changes found in the hemodynamic patterns and in particular in developing turbulence structures. Our findings and their implications were found to be similar to those arising in a tricuspid stenotic case, leading to increased turbulence and shear stresses in the ascending aorta, with possible weakening and bulging of the aortic wall leading to dilation and even aneurysm (Manchester et al. 2021).

Some limitations characterize the present work. First, we assumed rigid walls. Fluid-structure interaction simulations should be considered for future works to better assess the amount of turbulence developed in BAV and TAV cases. However, for the present work the assumption of rigid wall could be in our opinion acceptable as a first approximation since we are more interested in the comparison rather than the absolute quantification of turbulence. Second, only one representative case for each model (BAV and TAV) has been studied. More scenarios including also pathological cases (dilated, stenotic, ….) should be considered in future works. We also mention that the duration of the diastolic phase is slightly shorter than the physiological one, in comparison to the systolic phase. We also stress that we modified the flow curve taken from Avolio (1980) removing the negative portion of the flow curve and adjusted it to nullify negative values. As noticed, this should not affect the comparisons among the scenarios we proposed in this work; however this limitation will be overcome in future studies to better understand its suitability.

As a conclusion, blood flows in patient-specific aortas with TAV and BAV configurations, including leaflets, have been numerically simulated with the LES method using the σ-model to observe how the functional state of the aortic valve would affect the characteristics of flow hemodynamics. The high viscosity ratio and standard deviation representing turbulent flow, retrograde flow jets, and elevated WSS caused by valve regurgitation were observed. These results imply that ascending aortic flow patterns are significantly affected by aortic valve dysfunction. Furthermore, the bicuspid valve, which can produce turbulence in blood flow and a high WSS on the ascending aorta, can damage the valve over time and result in stenosis as well as other issues including regurgitation and an aortic aneurysm (Liu et al. 2018).

Disclosure statement

No potential conflict of interest was reported by the authors.

Funding

This work was supported by Türkiye Bilimsel ve Teknolojik Araştırma Kurumu.

References

Avolio A. 1980. Multi-branched model of the human arterial system. Med Biol Eng Comput. 18(6):709–718. doi:10.1007/BF02441895.

Barker AJ, Markl M, Bürk J, Lorenz R, Bock J, Bauer S, Schulz-Menger J, von Knobelsdorff-Brenkenhoff F. 2012. Bicuspid aortic valve is associated with altered wall shear stress in the ascending aorta. Circ Cardiovasc Imaging. 5(4):457–466. doi:10.1161/CIRCIMAGING.112.973370.

Benim AC, Gul F, Assmann A, Akhyari P, Lichtenberg A, Joos F. 2016. Validation of loss-coefficient based outlet boundary conditions for simulating aortic flow. J Mech Med Biol. 16(02):1650011. doi:10.1142/S0219519416500111.

Bennati L, Vergara C, Giambruno V, Fumagalli I, Corno AF, Quarteroni A, Puppini G, Luciani GB. 2023. An image-based computational fluid dynamics study of mitral regurgitation in presence of prolapse. Cardiovasc Eng Technol. 14(3):457–475. doi:10.1007/s13239-023-00665-3.

Bertagna L, Deparis S, Formaggia L, Forti D, Veneziani A. 2017. The LifeV library: engineering mathematics beyond the proof of concept. arXiv preprint arXiv:171006596.

Billiar K, Sacks M. 2000. Biaxial mechanical properties of the natural and glutaraldehyde treated aortic valve cusp—part i: experimental results. J Biomech Eng. 122(1):23–30. doi:10.1115/1.429624.

Bissell M, Hess A, Biasiolli L, Glaze S, Loudon M, Pitcher A, Davis A, Prendergast B, Markl M, Barker A, et al. 2013. Aortic dilation in bicuspid aortic valve disease: flow pattern is a major contributor and differs with valve fusion type. Circ Cardiovasc Imaging. 6(4):499–507. doi:10.1161/CIRCIMAGING.113.000528.

Bonomi D, Vergara C, Faggiano E, Stevanella M, Conti C, Redaelli A, Puppini G, Faggian G, Formaggia L, Luciani G. 2015. Influence of the aortic valve leaflets on the fluid-dynamics in aorta in presence of a normally functioning bicuspid valve. Biomech Model Mechanobiol. 14(6):1349–1361. doi:10.1007/s10237-015-0679-8.

Burris N, Hope M. 2015. Bicuspid valve-related aortic disease: flow assessment with conventional phase-contrast MRI. Acad Radiol. 22(6):690–696. doi:10.1016/j.acra.2015.01.010.

Cao K, Atkins S, McNally A, Liu J, Sucosky P. 2017. Simulations of morphotype-dependent hemodynamics in non-dilated bicuspid aortic valve aortas. J Biomech. 50:63–70. doi:10.1016/j.jbiomech.2016.11.024.

Cao K, Sucosky P. 2017. Computational comparison of regional stress and deformation characteristics in tricuspid and bicuspid aortic valve leaflets. Numer Methods Biomed Eng. 33(3):1–21. doi:10.1002/cnm.2798.

Cecconi M, Manfrin M, Moraca A, Zanoli R, Colonna P, Bettuzzi M, Moretti S, Gabrielli D, Perna G. 2005. Aortic dimensions in patients with bicuspid aortic valve without significant valve dysfunction. Am J Cardiol. 95(2):292–294. doi:10.1016/j.amjcard.2004.08.098.

Chandra S, Rajamannan N, Sucosky P. 2012. Computational assessment of bicuspid aortic valve wall-shear stress: implications for calcific aortic valve disease. Biomech Model Mechanobiol. 11(7):1085–1096. doi:10.1007/s10237-012-0375-x.

Chandran K, Vigmostad S. 2013. Patient-specific bicuspid valve dynamics: overview of methods and challenges. J Biomech. 46(2):208–216. doi:10.1016/j.jbiomech.2012.10.038.

Chnafa C, Mendez S, Nicoud F. 2016. Image-based simulations show important flow fluctuations in a normal left ventricle: what could be the implications? Ann Biomed Eng. 44(11):3346–3358. doi:10.1007/s10439-016-1614-6.

Conti CA, Della Corte A, Votta E, Del Viscovo L, Bancone C, De Santo LS, Redaelli A. 2010. Biomechanical implications of the congenital bicuspid aortic valve: a finite element study of aortic root function from in vivo data. J Thorac Cardiovasc Surg. 140(4):890–896.e2. doi:10.1016/j.jtcvs.2010.01.016.

Davies P, Remuzzi A, Gordon E, Dewey C, Gimbrone M. 1986. Turbulent fluid shear-stress induces vascular endothelial-cell turnover in vitro. Proc Natl Acad Sci U S A. 83(7):2114–2117. doi:10.1073/pnas.83.7.2114.

de Sa M, Moshkovitz Y, Butany J, David TE. 1999. Histologic abnormalities of the ascending aorta and pulmonary trunk in patients with bicuspid aortic valve disease: clinical relevance to the ross procedure. J Thorac Cardiovasc Surg. 118(4):588–594. doi:10.1016/S0022-5223(99)70002-4.

Faggiano E, Antiga L, Puppini G, Quarteroni A, Luciani G, Vergara C. 2013a. Helical flows and asymmetry of blood jet in dilated ascending aorta with normally functioning bicuspid valve. Biomech Model Mechanobiol. 12(4):801–813. doi:10.1007/s10237-012-0444-1.

Fedak P, Verma S, David T, Leask R, Weisel R, Butany J. 2002. Clinical and pathophysiological implications of a bicuspid aortic valve. Circulation. 106(8):900–904. doi:10.1161/01.cir.0000027905.26586.e8.

Fortini S, Espa S, Querzoli G, Cenedese A. 2015. Turbulence investigation in a laboratory model of the ascending aorta. J Turbul. 16(3):208–224. doi:10.1080/14685248.2014.982248.

Gårdhagen R, Lantz J, Carlsson F, Karlsson M. 2010. Quantifying turbulent wall shear stress in a stenosed pipe using large eddy simulation. J Biomech Eng. 132:061002.

Girdauskas E, Borger MA, Secknus MA, Girdauskas G, Kuntze T. 2011. Is aortopathy in bicuspid aortic valve disease a congenital defect or a result of abnormal hemodynamics? a critical reappraisal of a one-sided argument. Eur J Cardio-Thoracic Surg. 39(6):809–814. doi:10.1016/j.ejcts.2011.01.001.

Gülan U, Calen C, Duru F, Holzner M. 2016. Blood flow patterns and pressure loss in the ascending aorta: a comparative study on physiological and aneurysmal conditions. J Biomech. 30(1):67–85.

Guzzardi DG, Barker AJ, van Ooij P, Malaisrie SC, Puthumana JJ, Belke DD, Mewhort HE, Svystonyuk DA, Kang S, Verma S, et al. 2015. Valve-related hemodynamics mediate human bicuspid aortopathy: insights from wall shear stress mapping. J Am Coll Cardiol. 66(8):892–900. doi:10.1016/j.jacc.2015.06.1310.

Ha H, Ziegler M, Welander M, Bjarnegård N, Carlhäll C, Lindenberger M, Länne T, Ebbers T, Dyverfeldt P. 2018. Age-related vascular changes affect turbulence in aortic blood flow. Front Physiol. 9:36–46. doi:10.3389/fphys.2018.00036.

Hahn RT, Roman MJ, Mogtader AH, Devereux RB. 1992. Association of aortic dilation with regurgitant, stenotic and functionally normal bicuspid aortic valves. J Am Coll Cardiol. 19(2):283–288. doi:10.1016/0735-1097(92)90479-7.

Hope M, Hope T, Crook S, Ordovas K, Urbania T, Alley M, Higgins C. 2011. 4d flow cmr in assessment of valve-related ascending aortic disease. JACC Cardiovasc Imaging. 4(7):781–787. doi:10.1016/j.jcmg.2011.05.004.

Hope M, Hope T, Meadows A, Ordovas K, Urbania T, Alley M, Higgins C. 2010. Bicuspid aortic valve: four-dimensional mr evaluation of ascending aortic systolic flow patterns. Radiology. 255(1):53–61. doi:10.1148/radiol.09091437.

Hsu CH, Nguyen BS, Vu HH. 2011. Hemodynamics and mechanical behaviors of aortic heart valves: a numerical evaluation. In: 2011 4th International Conference on Biomedical Engineering and Informatics (BMEI); vol. 2. p. 1101–1105. doi:10.1109/BMEI.2011.6098417.

Jermihov PN, Jia L, Sacks MS, Gorman RC, Gorman JH, Chandran KB. 2011. Effect of geometry on the leaflet stresses in simulated models of congenital bicuspid aortic valves. Cardiovasc Eng Technol. 2(1):48–56. doi:10.1007/s13239-011-0035-9.

Kara R, Çağlar M. 2018. Çinlar subgrid scale model for large eddy simulation. Appl Math Comput. 322:89–99. doi:10.1016/j.amc.2017.11.033.

Kheradvar A, Pedrizzetti G. 2012. Vortex formation in the cardiovascular systems. London: Springer-Verlag. doi:10.1007/978-1-4471-2288-3.

Kimura N, Nakamura M, Komiya K, Nishi S, Yamaguchi A, Tanaka O, Misawa Y, Adachi H, Kawahito K.,. 2017. Patient-specific assessment of hemodynamics by computational fluid dynamics in patients with bicuspid aortopathy. J Thorac Cardiovasc Surg. 153(4):S52–S62.e3. doi:10.1016/j.jtcvs.2016.12.033.

Lancellotti R, Vergara C, Valdettaro L, Bose S, Quarteroni A. 2017. Large eddy simulations for blood dynamics in realistic stenotic carotids. Int J Numer Meth Biomed Eng. 33(11):e2868.

Lantz J, Gårdhagen R, Karlsson M. 2012. Quantifying turbulent wall shear stress in a subject specific human aorta using large eddy simulation. Med Eng Phys. 34(8):1139–1148. doi:10.1016/j.medengphy.2011.12.002.

Liu T, Xie M, Lv Q, Li Y, Fang L, Zhang L, Deng W, Wang J. 2018. Bicuspid aortic valve: an update in morphology, genetics, biomarker, complications, imaging diagnosis and treatment. Front Physiol. 9(9):1921. doi:10.3389/fphys.2018.01921.

Mahadevia R, Barker AJ, Schnell S, Entezari P, Kansal P, Fedak PWM, Malaisrie SC, McCarthy P, Collins J, Carr J, et al. 2014. Bicuspid aortic cusp fusion morphology alters aortic 3d outflow patterns, wall shear stress and expression of aortopathy. Circulation. 129(6):673–682. doi:10.1161/CIRCULATIONAHA.113.003026.

Malota Z, Glowacki J, Kukulski T, Sadowski W. 2013. Impact of geometric changes in a dilated aorta with a bicuspid aortic valve on blood flow disturbances a numerical modelling study. Kardiochirurgia I Torakochirurgia Polska. 10(2):139–148.

Manchester EL, Pirola S, Salmasi MY, O'Regan DP, Athanasiou T, Xu XY. 2021. Analysis of turbulence effects in a patient-specific aorta with aortic valve stenosis. Cardiovasc Eng Technol. 12(4):438–453. doi:10.1007/s13239-021-00536-9.

Marom G, Kim H, Rosenfeld M, Raanani E, Haj-Ali R. 2013. Fully coupled fluid–structure interaction model of congenital bicuspid aortic valves:effect of asymmetry on hemodynamics. Med Biol Eng Comput. 51(8):839–848. doi:10.1007/s11517-013-1055-4.

McNally A, Madan A, Sucosky P. 2017. Morphotype-dependent flow characteristics in bicuspid aortic valve ascending aortas: a benchtop particle image velocimetry study. Front Physiol. 8:44. doi:10.3389/fphys.2017.00044.

Moireau P, Xiao N, Astorino M, Figueroa C, Chapelle D, Taylor C, Gerbeau J. 2012. External tissue support and fluid structure simulation in blood flows. Biomech Model Mechanobiol. 11(1–2):1–18. doi:10.1007/s10237-011-0289-z.

Morbiducci U, Ponzini R, Rizzo G, Cadioli M, Esposito A, Montevecchi F, Redaelli A. 2011. Mechanistic insight into the physiological relevance of helical blood flow in the human aorta: an in vivo study. Biomech Model Mechanobiol. 10(3):339–355. doi:10.1007/s10237-010-0238-2.

Nathan DP, Xu C, Plappert T, Desjardins B, Gorman JH, Bavaria JE, Gorman RC, Chandran KB, Jackson BM. 2011. Increased ascending aortic wall stress in patients with bicuspid aortic valves. Ann Thorac Surg. 92(4): 1384–1389. doi:10.1016/j.athoracsur.2011.04.118.

Nerem R, Seed W. 1972. An in vivo study of aortic flow disturbances. Cardiovasc Res. 6(1):1–14. doi:10.1093/cvr/6.1.1.

Nicoud F, Toda HB, Cabrit O, Bose S, Lee J. 2011. Using singular values to build a subgrid-scale model for large eddy simulations. Physics of Fluids. 23(8):085106. doi:10.1063/1.3623274.

Nygaard H, Paulsen P, Hasenkam J, Pedersen E, Rovsing P. 1994. Turbulent stresses downstream of three mechanical aortic valve prostheses in human beings. J Thorac Cardiovasc Surg. 107(2):438–446.

Oliveira D, Rosa S, Tiago J, Ferreira R, Agapito A, Sequeira A. 2019. Bicuspid aortic valve aortopathies: an hemodynamics characterization in dilated aortas. Comput Methods Biomech Biomed Engin. 22(8):815–826. doi:10.1080/10255842.2019.1597860.

Pasta S, Rinaudo A, Luca A, Pilato M, Scardulla C, Gleason T, Vorp D. 2013. Difference in hemodynamic and wall stress of ascending thoracic aortic aneurysms with bicuspid and tricuspid aortic valve. J Biomech. 46(10):1729–1738. doi:10.1016/j.jbiomech.2013.03.029.

Richards KE, Deserranno D, Donal E, Greenberg NL, Thomas JD, Garcia MJ. 2004. Influence of structural geometry on the severity of bicuspid aortic stenosis. Am J Physiol Heart Circ Physiol. 287(3):H1410–1416.

Rinaudo A, Pasta S. 2014. Regional variation of wall shear stress in ascending thoracic aortic aneurysms. Proc Inst Mech Eng H. 228(6):627–638. doi:10.1177/0954411914540877.

Sagaut P, Meneveau C, editors. 2006. Large eddy simulation for incompressible flows. Berlin: Springer. Scientific Computation.

Saikrishnan N, Mirabella L, Yoganathan A. 2015. Bicuspid aortic valves are associated with increased wall and turbulence shear stress levels compared to trileaflet aortic valves. Biomech Model Mechanobiol. 14(3):577–588. doi:10.1007/s10237-014-0623-3.

Seaman C, Akingba A, Sucosky P. 2014. Steady flow hemodynamic and energy loss measurements in normal and simulated calcified tricuspid and bicuspid aortic valves. J Biomech Eng. 136:1–11.

Shan Y, Li J, Wang Y, Wu B, Barker AJ, Markl M, Wang C, Wang X, Shu X. 2017. Aortic shear stress in patients with bicuspid aortic valve with stenosis and insufficiency. J Thorac Cardiovasc Surg. 153(6):1263–1272.e1.,. doi:10.1016/j.jtcvs.2016.12.059.

Sievers H, Sievers H. 2011. Aortopathy in bicuspid aortic valve diseasegenes or hemodynamics? or scylla and charybdis? Eur J Cardiothorac Surg. 39(6):803–804. doi:10.1016/j.ejcts.2011.02.007.

Stein P, Sabbah H. 1976. Turbulent blood flow in the ascending aorta of humans with normal and diseased aortic valves. Circ Res. 39(1):58–65. doi:10.1161/01.res.39.1.58.

Steinman D. 2002. Image-based computational fluid dynamics modeling in realistic arterial geometries. Ann Biomed Eng. 30(4):483–497. doi:10.1114/1.1467679.

Tadros T, Klein M, Shapira O. 2009. Ascending aortic dilatation associated with bicuspid aortic valve. pathophysiology, molecular biology, and clinical implications. Circulation. 119(6):880–890. doi:10.1161/CIRCULATIONAHA.108.795401.

Tan F, Wood N, Tabor G, Xu X. 2011. Comparison of les of steady transitional flow in an idealized stenosed axisymmetric artery model with a rans transitional model. J Biomech Eng. 133:051001.

Torii R, Kalantzi M, Theodoropoulos S, Sarathchandra P, Xu X, Yacoub M. 2013. Predicting impending rupture of the ascending aorta with bicuspid aortic valve, spatio temporal flow and wall shear stress. J Am Coll Cardiol Img. 6(9):1017–1019. doi:10.1016/j.jcmg.2013.02.012.

Trigui A, Chiekh MB, Béra JC, Gilles B. 2021. Experimental and numerical investigation of pulsed flows in a severe aortic stenosed model. Med Eng Phys. 90:33–42. doi:10.1016/j.medengphy.2021.02.006.

van Ooij P, Potters W, Collins J, Carr M, Carr J, Malaisrie S, Fedak P, McCarthy P, Markl M, Barker A. 2015. Characterization of abnormal wall shear stress using 4d flow mri in human bicuspid aortopathy. Ann Biomed Eng. 43(6):1385–1397. doi:10.1007/s10439-014-1092-7.

Varghese S, Frankel S, Fischer P. 2008. Modeling transition to turbulence in eccentric stenotic flows. J Biomech Eng. 130(1):014503. doi:10.1115/1.2800832.

Vergara C, Van D, Quadrio M, Formaggia L, Domanin M. 2017. Large eddy simulations of blood dynamics in abdominal aortic aneurysms. Med Eng Phys. 47:38–46. doi:10.1016/j.medengphy.2017.06.030.

Vergara C, Viscardi F, Antiga L, Luciani GB. 2012. Influence of bicuspid valve geometry on ascending aortic fluid dynamics: a parametric study. Artif Organs. 36(4): 368–378. doi:10.1111/j.1525-1594.2011.01356.x.

Viscardi F, Vergara C, Antiga L, Merelli S, Veneziani A, Puppini G, Faggian G, Mazzucco A, Luciani GB.,. 2010. Comparative finite element model analysis of ascending aortic flow in bicuspid and tricuspid aortic valve. Artif Organs. 34(12):1114–1120. doi:10.1111/j.1525-1594.2009.00989.x.

Wendell D, Samyn M, Cava J, Krolikowski M, LaDisa J. 2016. The impact of cardiac motion on aortic valve flow used in computational simulations of the thoracic aorta. J Biomech Eng. 138(9):091001.

Wittberg P, van Wyk S, Fuchs L, Gutmark E, Backeljauw P, Gutmark-Little I. 2016. Effects of aortic irregularities on blood flow. Biomech Model Mechanobiol. 15(2):345–360. doi:10.1007/s10237-015-0692-y.

Xu L, Yang T, Yin L, Kong Y, Vassilevski Y, Liang F. 2020. Numerical simulation of blood flow in aorta with

dilation: a comparison between laminar and les modeling methods. Heart Vessels. 124(2):509–526. doi:10.32604/cmes.2020.010719.

Youssefi P, Gomez A, He T, Anderson L, Bunce N, Sharma R, Figueroa C, Jahangiri M. 2017. Patient-specific computational fluid dynamics assessment of aortic hemodynamics in a spectrum of aortic valve pathologies. J Thorac Cardiovasc Surg. 153(1):8–20.e3. doi:10.1016/j.jtcvs.2016.09.040.

Zhang Q, Gao B, Chang Y. 2018. Helical flow component of left ventricular assist devices (lvads) outflow improves aortic hemodynamic states. Med Sci Monit. 24:869–879. doi:10.12659/msm.905940.